The Ras-RasGAP Complex: Structural Basis for GTPase Activation and Its Loss in Oncogenic Ras Mutants

Klaus Scheffzek, Mohammad Reza Ahmadian, Wolfgang Kabsch, Lisa Wiesmüller,* Alfred Lautwein,† Frank Schmitz, Alfred Wittinghofer‡

The three-dimensional structure of the complex between human H-Ras bound to guanosine diphosphate and the guanosine triphosphatase (GTPase)–activating domain of the human GTPase-activating protein $p120^{GAP}$ (GAP-334) in the presence of aluminum fluoride was solved at a resolution of 2.5 angstroms. The structure shows the partly hydrophilic and partly hydrophobic nature of the communication between the two molecules, which explains the sensitivity of the interaction toward both salts and lipids. An arginine side chain (arginine-789) of GAP-334 is supplied into the active site of Ras to neutralize developing charges in the transition state. The switch II region of Ras is stabilized by GAP-334, thus allowing glutamine-61 of Ras, mutation of which activates the oncogenic potential, to participate in catalysis. The structural arrangement in the active site is consistent with a mostly associative mechanism of phosphoryl transfer and provides an explanation for the activation of Ras by glycine-12 and glutamine-61 mutations. Glycine-12 in the transition state mimic is within van der Waals distance of both arginine-789 of GAP-334 and glutamine-61 of Ras, and even its mutation to alanine would disturb the arrangements of residues in the transition state.

The Ras proteins H-, K-, and N-Ras are central regulators of cellular signal transduction processes leading to cell growth and differentiation. They are molecular switches that in the resting cell are in the guanosine diphosphate (GDP)–bound inactive state. In response to receptor protein tyrosine kinases or other growth factor–dependent stimuli, these Ras proteins become activated by binding guanosine triphosphate (GTP). In the GTP-bound active state, they interact with and activate downstream targets. GTP hydrolysis mediated by Ras completes the GTPase cycle (*1*).

The conformational state of Ras is regulated by two kinds of proteins, guanine nucleotide exchange factors (GEFs) and GTPase-activating proteins (GAPs) (*2*). GEFs such as Sos or Cdc25 increase the dissociation rate of guanine nucleotides, allowing GTP, which is more prevalent in the cell, to bind Ras. GAPs inactivate Ras by accelerating the slow intrinsic rate of GTP hydrolysis by several orders of magnitude. Five mammalian GAPs for Ras have been described (*2*), including $p120^{GAP}$, the prototype for this class of proteins (*3*), and neurofibromin, the product of the type I neurofibromatosis (*NF1*) gene (*4*, *5*).

Oncogenic mutants of Ras are found in about 25 to 30% of human tumors. They have an impaired intrinsic GTPase and are insensitive to GAPs, and thus are unable to switch off the transmitted signal. Because of the action of the negative regulator GAP, wild-type Ras is found in the inactive GDP-bound state in unstimulated cells, whereas oncogenic Ras remains GTP-bound (*1*).

The mechanism by which GAPs accelerate the GTPase reaction has been a matter of debate (*6*, *7*). In one model, Ras itself is an efficient GTPase, and GAP induces the attainment of a GTPase-competent conformation indirectly by catalyzing a rate-limiting isomerization reaction. Conflicting evidence for such an isomerization reaction catalyzed by GAP has been presented (*8*). In another model, the actual chemical cleavage step is modified by GAP directly, most likely by GAP supplying residues for GTP hydrolysis on Ras and thereby stabilizing the transition state of the reaction. In support of this, RasGAPs (Ras-specific GAPs) have been found to stabilize binding of aluminum fluoride to Ras·GDP (*9*), forming a ternary complex that is believed to mimic the transition state of the GTPase reaction (*10*). Stoichiometric amounts of GAP are needed for this effect (*9*).

The catalytic fragment of $p120^{GAP}$, termed GAP-334, is a purely helical molecule consisting of two domains, the larger of which contains all residues conserved among RasGAPs. On the basis of much biochemical and genetic data, a model was proposed of how Ras might interact with GAP-334 (*11*). We now have solved the crystal structure of the complex between GAP-334 and Ras·GDP in the presence of aluminum fluoride.

Structure of the Ras·RasGAP complex. Crystals were obtained from solutions of Ras·GDP and GAP-334 mixed with aluminum fluoride (*12*). We determined the structure by the molecular replacement

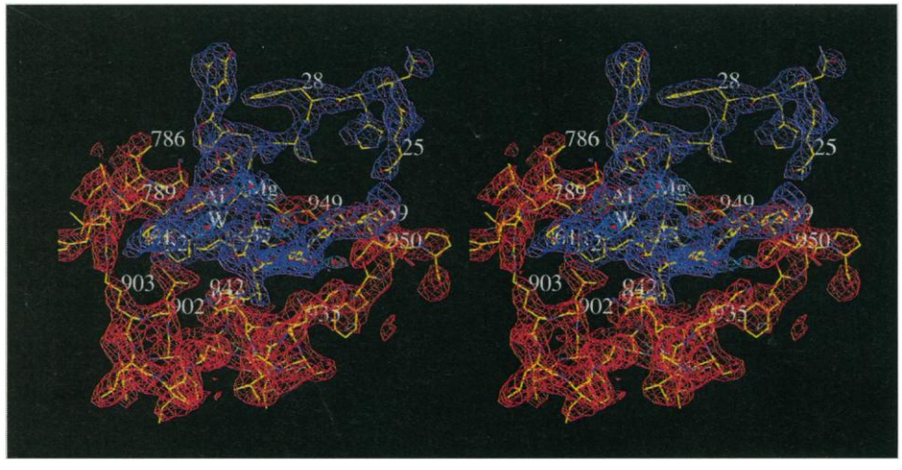

Fig. 1. Stereo view of a segment of the $2F_o - F_c$ electron density map (contoured at 1.2σ) covering the active site region in the complex, with Ras in blue, GAP-334 in red, and waters in light blue.

K. Scheffzek, M. R. Ahmadian, L. Wiesmüller, A. Lautwein, F. Schmitz, and A. Wittinghofer are at the Max-Planck-Institut für molekulare Physiologie, Abteilung Strukturelle Biologie, Rheinlanddamm 201, 44139 Dortmund, Germany. W. Kabsch is at the Max-Planck-Institut für medizinische Forschung, Jahnstrasse 29, 69120 Heidelberg, Germany.

*Present address: Heinrich Pette Institut für experimentelle Virologie und Immunologie an der Universität Hamburg, Martinistrasse 52, 20251 Hamburg, Germany.
†Present address: Chester Beatty Laboratories, Fulham Road, London SW3 6JB, England.
‡To whom correspondence should be addressed. E-mail: Alfred.Wittinghofer@mpi-dortmund.mpg.de

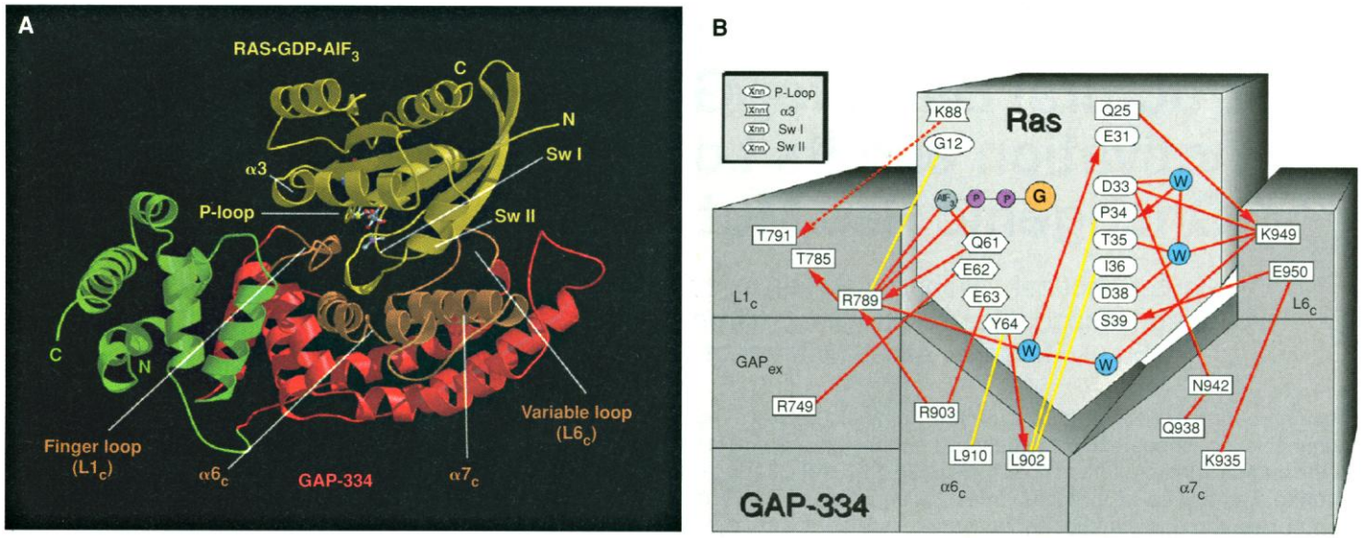

Fig. 2. The complex between GAP-334 and Ras. (**A**) Ribbon representation of the complex model drawn with Molscript (*52*) and Raster3D (*53*) according to the assignment of secondary structure elements obtained with the program DSSP (*54*). The extra and catalytic domains of GAP-334 are shown in green and red (respectively), regions of GAP contacting Ras in light brown, Ras in yellow, and GDP and AlF_3 as ball-and-stick models. Regions involved in the interface are labeled, Sw I and Sw II indicating the switch regions, C the COOH-terminal, and N the NH_2-terminal. (**B**) Schematic drawing with selected interactions. Polar interactions between individual residues of GAP-334 and Ras are shown as red lines for interactions of side chains, and as red arrows for contacts from side chain to main chain atoms, where the arrowhead marks the residue contributing the main chain group. Yellow lines indicate van der Waals or hydrophobic interactions. Some water molecules (marked W) from the interface region are included. Residues belonging to the interacting regions of Ras indicated in (A) are denoted with specified boxes, as indicated. Interaction between Lys^{88} and Thr^{791} is shown by a dashed arrow, because the electron density in this region is presently not of sufficient quality to unambiguously define the contact. Amino acid abbreviations are in (*55*).

method using the coordinates of GAP-334 (*11*) and Ras (*13*) as search models. Both rotation and translation functions, calculated with the program X-PLOR (*14*), showed unique peaks for the GAP-334 and Ras models. The electron density map based on the phases derived from the GAP model after rigid body refinement showed clear density for the Ras molecule that was subsequently adjusted manually in the map. Rigid body and initial Powell minimization resulted in an electron density map that showed a strong peak for the bound nucleotide that was incorporated as GDP into the complex model. After rebuilding of residues 46 to 54 and 61 to 66 in Ras and of residues 830 to 839 and 947 to 952 in GAP-334, another round of positional refinement was done, yielding an R factor of 32% (R_{free} = 37%). Local errors were corrected by subsequent rounds of alternate model building and positional and temperature factor refinement, along with simulated annealing, including bulk solvent correction; water molecules were added in $F_o - F_c$ maps [programs O (*15*) and X-PLOR 3.8 (*14*)]. A maximum of electron density in the position usually occupied by the γ-phosphate present in all maps during refinement was interpreted as aluminum fluoride. From the outline in $F_o - F_c$ maps it appeared to be a trigonal AlF_3 moiety rather than a tetragonal AlF_4^-, as observed in the structures of activated α subunits of the heterotrimeric guanine nucleotide–binding proteins $G\alpha_{i1}$ and $G\alpha_t$ (*10*). Residues 981 to 990 are ill-defined in the electron density and were modeled stereochemically. Our model comprises residues 718 to 1037 of GAP-334, residues 1 to 166 of H-Ras, GDP, AlF_3, Mg^{2+}, and 35 water molecules. The refinement is summarized in Table 1, and a representative part of the electron density map is shown in Fig. 1.

A ribbon representation and a schematic drawing of the complex are shown in Fig. 2.

Table 1. Summary of crystallographic analysis.

	Search model	
	GAP-334(718–1042)	H-Ras(1–166)
Data collection		
Resolution limit (Å)	2.4	
Total reflections (*N*)	35,339	
Unique reflections (*N*)	15,811	
Completeness (%)	81	
R_{sym} (%)*	6.6	
Molecular replacement		
Resolution range (Å)	15 to 4	15 to 4
Θ_1, Θ_2, Θ_3 rotation† (degrees)	18.6, 36.8, 256	31.6, 89.8, 250.2
x, *y*, *z* translation‡	0.059, 0.0, 0.273	0.36, 0.0, 0.49
Refinement		
Resolution (Å)	30 to 2.5	
Number of unique reflections	15,548	
R_{cryst} (%)§	23.3	
R_{free} (%)‖	32.3	
rmsd bond length (Å)	0.007	
rmsd bond angles (degrees)	1.27	

*$R_{sym} = \Sigma|I_{hi} - I_h|/\Sigma I_{hi}$, where I_{hi} is the scaled intensity of the *i*th symmetry-related observation of reflection *h* and I_h is the mean value. †Eulerian angles Θ_1, Θ_2, Θ_3, as defined in X-PLOR. ‡Fractional coordinates *x*, *y*, *z* as obtained by X-PLOR. §$R_{cryst} = \Sigma_h|F_{oh} - F_{ch}|/\Sigma_h F_{oh}$, where F_{oh} and F_{ch} are the observed and calculated structure factor amplitudes for reflection *h*. ‖Value of R_{cryst} for 10% randomly chosen reflections not included in the refinement.

The overall structures of GAP-334 and Ras are similar to those of the isolated molecules. The most significant differences are seen in the switch II region of Ras and the loop $L6_c$ of GAP-334. The values for the root-mean-square deviation (rmsd) for superimposition of corresponding Cα atoms are 0.9 Å for GAP-334 and 0.54 Å for Ras, using free GAP-334 (*11*) and Ras·GppNHp (*13*) for the comparison. The orientation of the two proteins in the complex structure is similar to that of our earlier docking model [figure 4 in (*11*)]. Activated Ras binds in the shallow groove of the central catalytic domain GAP_c of GAP-334, with the tip of its triangular shape penetrating most deeply into the groove. A large amount of solvent-accessible surface area (3145 $Å^2$) becomes buried in the interface during complex formation (*16*). Consistent with numerous mutational studies, residues of the phosphate-binding (P-) loop (residues 10 to 16), switch regions I (30 to 37) and II (60 to 76), and possibly helix α3 (87 to 98) on Ras (Fig. 2) participate in the interaction (*17–19*). The switch regions of Ras have been defined as the regions that change their structure upon transition from the GTP- to the GDP-bound state (*20*). On the GAP side, helices $\alpha6_c$ and $\alpha7_c$ and loops $L1_c$ and $L6_c$ are involved in the interaction with Ras (Figs. 2 and 3). We call $L1_c$ the finger loop because it points into the active site and $L6_c$ the variable loop because its length is variable in the structure-based alignment (Fig. 3, see below). In contrast to the complex of the Ras-related Rap1A·GppNHp with the Ras-binding domain of the protein kinase Raf, which shows many strong polar hydrogen bonds and salt bridges between the two proteins (*21*), the interface of the Ras·RasGAP complex consists of weak van der Waals interactions and a number of polar interactions also involving several water molecules. Because the affinity between GAP-334 and Ras·GTP (5 μM) decreases strongly with increasing salt concentration, polar interactions appear to predominate in the affinity of GAP-334 for Ras (*22*). The structure suggests that the extra domain of GAP-334, GAP_{ex}, is dispensable for Ras-RasGAP interaction, consistent with studies on neurofibromin that showed that a 230-residue fragment corresponding to the catalytic domain of GAP-334 (red/brown in Fig. 2A) is sufficient for GTPase activation (*23*).

Contact with the switch regions of Ras. Switch I overlaps with the Ras effector region (*24*). It interacts predominantly with the central helices $\alpha6_c$ and $\alpha7_c$ and with the variable loop. Hydrophobic interactions are formed by the invariant Leu^{902} and Leu^{910} on $\alpha6_c$ of GAP and by Pro^{34}, Ile^{36}, Tyr^{32}, and Tyr^{64} of Ras (Figs. 2 and 4A). These interactions are presumably the target of inhibitory lipids such as phosphatidic acid and arachidonic acid (*25, 26*), the latter of which inhibits the Ras-RasGAP interaction in a partly competitive mode with respect to Ras·GTP (*27*). The partly hydrophobic nature of the interface might also explain the finding that the oncogenic mutation Gln^{61}→Leu in Ras, although unable to hydrolyze GTP efficiently, has a higher affinity than the wild type for either GAP-334 or neurofibromin (*26, 28–30*), and explain why apparently small perturbations such as the mutation Leu^{902}→Ile strongly inhibit catalysis (*29, 30*).

Switch I contains five acidic residues, Asp^{30}, Glu^{31}, Asp^{33}, Glu^{37}, and Asp^{38}, that create a negatively charged surface patch used for interaction with effectors (*21*) and with GAP-334 (Figs. 2 and 4, A and B). Lysine-949, located on the tip of a conspicuously exposed part of loop $L6_c$, points into the highly negatively charged surface patch. Whereas the side chains of Asp^{30}, Glu^{31}, and Glu^{37} are not directly involved in the interaction, Asp^{33} and Asp^{38} are oriented toward Lys^{949}, with only Asp^{33} making a direct contact and Asp^{38} and Thr^{35} making water-mediated polar contacts, which is mostly consistent with mutational studies (*17, 26, 31*).

From the invariant residues on helix $\alpha7_c$, only Asn^{942} directly contacts Ras. It forms a hydrogen bond with Asp^{33} of Ras, and its own orientation is stabilized by the carbonamide group of Gln^{938} (Figs. 2B and 4B). Lysine-935 forms an intramolecular salt bridge with Glu^{950} in loop $L6_c$, whose carboxylate group also contacts the main chain amide group of Ser^{39} of Ras (Fig. 4B). Lysine-1423 in neurofibromin (Lys^{935} in $p120^{GAP}$) is mutated to Glu or Gln in neurofibromas and solid tumors (*32*), and it is thought to be important for catalysis because GAP activity is reduced in such mutants, with conflicting results on its affinity for Ras (*32, 33*). On the basis of the intramolecular salt bridge between Lys^{935} and Glu^{950}, it appears unlikely that Lys^{935} is directly involved in catalysis or binding. One would postulate instead that most of its mutations should destabilize the protein, consistent with experimental findings on the Lys^{1423}→Met mutation in neurofibromin (*34*).

Two consecutive residues in loop $L6_c$, Lys^{949} and Glu^{950}, form a bifurcated clamp that fixes helix $\alpha7_c$ and the effector loop of Ras, and these residues appear to be of crucial importance for complex formation with Ras (Fig. 4B). We are proposing a structure-based alignment (Fig. 3) where the KE-motif (K is Lys and E is Glu) is

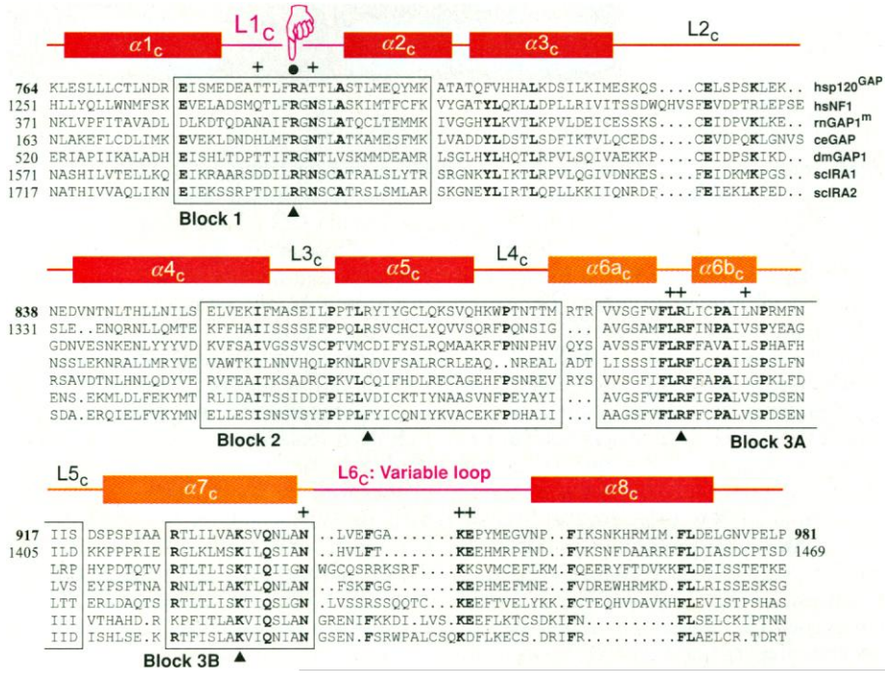

Fig. 3. Sequence alignment of the catalytic domain of RasGAPs from the indicated organisms, together with secondary structure assignment according to the program DSSP (*54*). hs, *Homo sapiens*; rn, *Rattus norvegicus*; ce, *Caenorhabditis elegans*; dm, *Drosophila melanogaster*; sc, *Saccharomyces cerevisiae*; IRA1 and IRA2 are yeast homologs of RasGAPs. Residues participating in catalysis are marked as closed circles, residues involved in Ras-RasGAP interaction as crosses, and residues that have been found mutated in neurofibromin from patients with type I neurofibromatosis and solid tumors as closed triangles. Amino acid abbreviations are in (*55*).

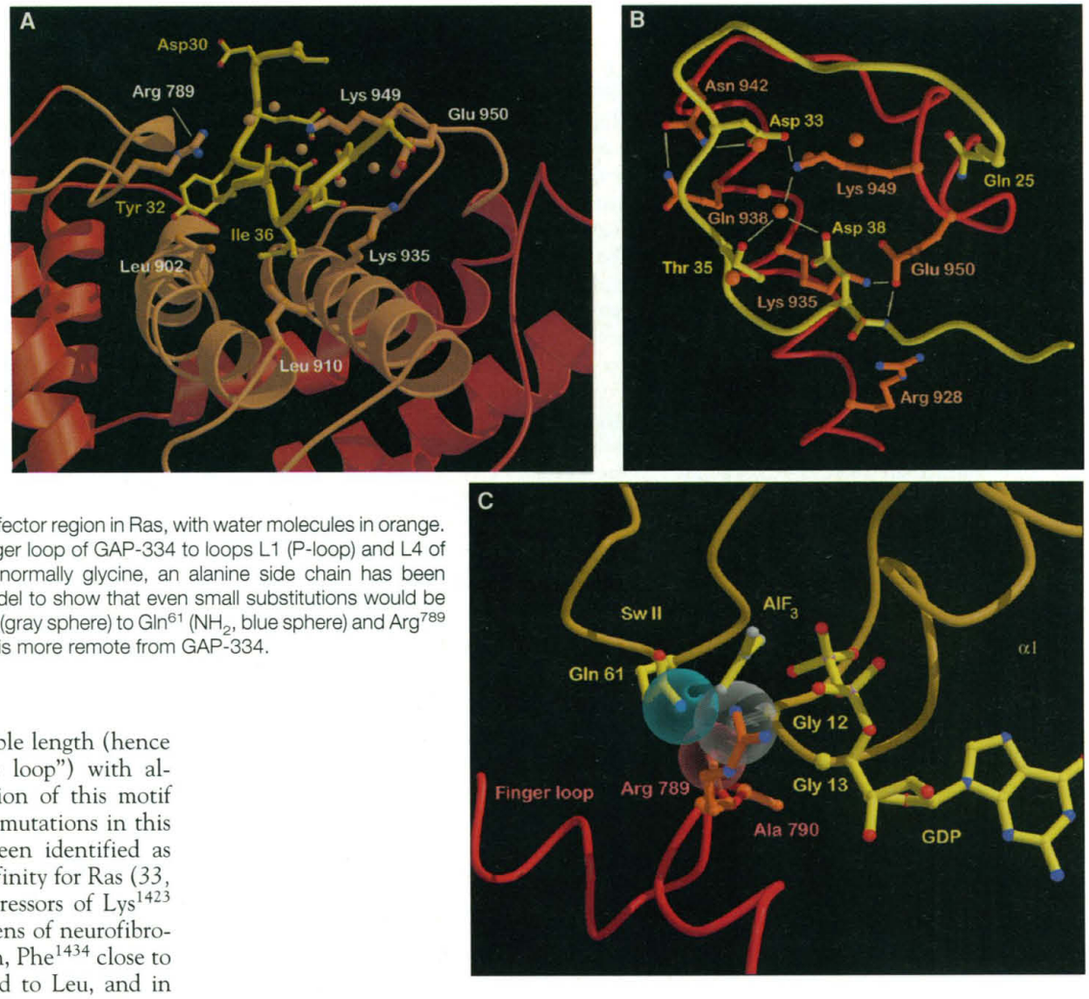

Fig. 4. Details of the interaction of Ras with GAP-334. (**A**) Residues 32 to 39 from the effector region of Ras, with side chains shown as ball-and-stick models (in yellow), contact GAP-334 (ribbon colored red and light brown as in Fig. 2A) in the vicinity of helices $\alpha 6_c$ and $\alpha 7_c$. Selected side chains of GAP-334 are shown as ball-and-stick models with Arg^{789} and Lys^{949} penetrating into the effector region from opposite sides, similar to the view in Fig. 1. Water molecules are light brown spheres. (**B**) Interaction of helix $H\alpha 7_c$ and the variable loop including the KE-motif of GAP-334 with part of the effector region in Ras, with water molecules in orange. (**C**) Close approach of the finger loop of GAP-334 to loops L1 (P-loop) and L4 of Ras. In position 12 of Ras, normally glycine, an alanine side chain has been introduced (gray) into the model to show that even small substitutions would be within van der Waals distance (gray sphere) to Gln^{61} (NH_2, blue sphere) and Arg^{789} (CO, red sphere). Glycine-13 is more remote from GAP-334.

situated in a loop of variable length (hence the designation "variable loop") with almost complete conservation of this motif and other residues. Point mutations in this loop have consistently been identified as mutants with increased affinity for Ras (*33*, *35*) or as intragenic suppressors of Lys^{1423} mutations in genetic screens of neurofibromin: In one such mutation, Phe^{1434} close to the KE-motif was mutated to Leu, and in the other, Lys^{1436} of the KE-motif itself was replaced by Arg (*35*).

Switch II comprises loop L4 and helix α2 in Ras. In contrast to the structures of isolated Ras where L4 appears highly mobile (*13*, *20*, *36*), this region is well defined in the complex with GAP-334. Residues 61 to 63 are arranged in a short 3_{10} helix preceding α2. Tyrosine-64 participates in the formation of the hydrophobic interface between Ras and GAP-334 and forms a polar contact with the main chain carbonyl group of Leu^{902}, consistent with the observation that it can be mutated to Phe but not to Glu without affecting Ras-RasGAP interaction (*17*). Interactions between Glu^{62} and Arg^{749} or between Glu^{63} and Arg^{903} may contribute to the stabilization of switch II. Glutamine-61 is essential for GTP hydrolysis: Its mutation to any other amino acid (except Glu) blocks Ras-mediated GTP hydrolysis (*18*, *19*, *26*, *37*, *38*) and leads to tumor formation. In Gα proteins in the GDP·AlF_4^- conformation, the Gln^{61} homolog stabilizes the transition state of the GTPase reaction (*10*), and a similar role was suggested for Gln^{61} of Ras (*39*). In the complex with GAP-334, Gln^{61} points toward the phosphate chain of the nucleotide and is stabilized in its orientation by a hydrogen bond with the main chain carbonyl group of the invariant Arg^{789}. The temperature factor distribution shows a local minimum for the L4 region (*40*), suggesting that binding of GAP to Ras results in stabilization of switch II.

Structural basis for oncogenicity of Gly^{12} mutants. Glycine-12 of the P-loop is critical for oncogenic activation of Ras because any mutation of this residue [except Gly^{12}→Pro (G12P)] activates the oncogenic potential of Ras (*41*). Ras(G12P), although insensitive to GAP, does not have transforming abilities, presumably because its intrinsic rate of GTP hydrolysis is slightly increased (*6*, *22*, *42*). No consistent explanation has so far been put forward to explain the defect in both the intrinsic and GAP-accelerated GTP hydrolysis of Gly^{12} mutants, although some have more obvious rearrangements of the active site (*28*, *43*). In the structure of the complex, Gly^{12} contacts the loop $L1_c$ region of GAP-334. The main chains approach each other, the closest encounter being a van der Waals contact between the Cα atom of Gly^{12} and the main chain CO of Arg^{789} (Fig. 4C). This mode of interaction imposes constraints on the space that may be filled by amino acids in position 12 of Ras and provides an explanation for the block in GAP-accelerated GTP hydrolysis. Although the interaction with GAP has not been investigated for all Gly^{12} mutants, it appears from the structure that even replacement with alanine would be highly unfavorable, leading to steric clashes with the main chain of Arg^{789} and with the side chain NH_2 of Gln^{61} (*31*). Glycine-12 mutants of Ras bind to GAP with an affinity similar to that of the wild type (*38*) without subsequent GTP hydrolysis. This suggests that the close neighborhood of Arg^{789} and Gly^{12} is not as crucial for the Ras·GTP·GAP ground state as for the transition state.

The active site and catalytic mechanism. GDP is bound in a mode similar to that observed in isolated Ras·GDP or Ras·GppNHp complexes, with Mg^{2+} present in the expected position (*13*, *20*).

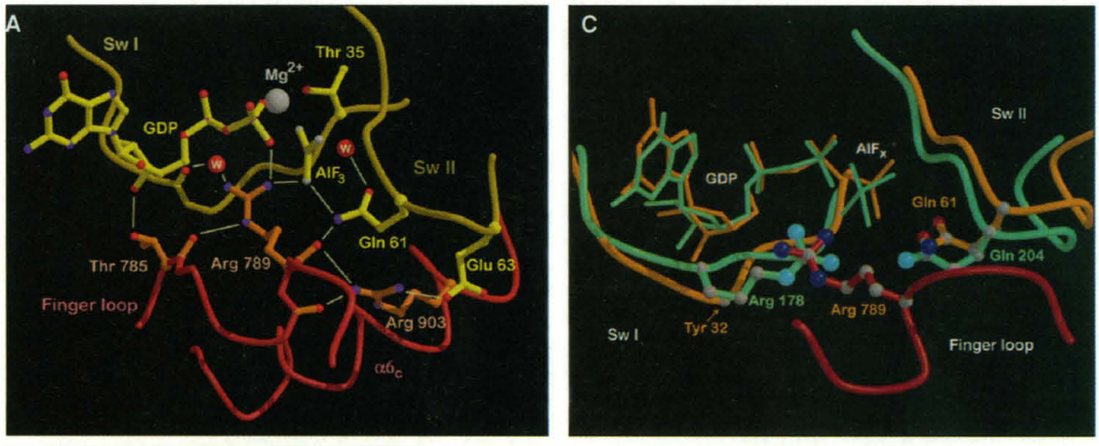

Fig. 5. Structural (**A**) and schematic (**B**) view of the active site, with the important elements of catalysis. (**C**) Superposition of the active site of $G\alpha_{i1}$·GDP·AlF_4^- (*10*) (green) and the Ras·GDP·AlF_3·GAP-334 (light brown/red) complexes (aligned by the G domains).

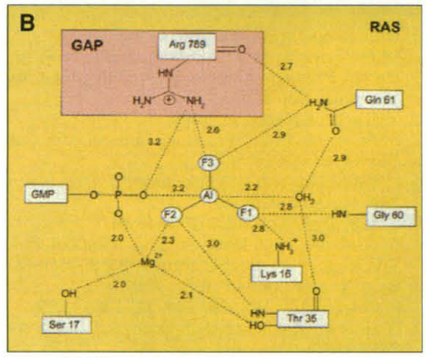

The 3′-OH group of the ribose that is exposed in isolated Ras is hydrogen bonded to the hydroxyl group of Thr^{785}. Aluminum fluoride, modeled as AlF_3, appears to be in an orientation such that the fluoride ligands contact Mg^{2+}, Thr^{35} (NH), Lys^{16} (NH_3^+), Gln^{61}(NH_2), and most significantly for the catalytic mechanism, the positively charged guanidinium group of Arg^{789} (Fig. 5, A and B). This residue in loop $L1_c$ is the postulated arginine finger (hence the designation "finger loop"), which participates in catalysis, consistent with mutational analysis (*31*). It points into the active site, is additionally stabilized by interaction with Thr^{785} (CO) (Fig. 5A), and communicates with Lys^{949} of the KE-motif through two water molecules, one of which contacts the main chain carbonyl group of Glu^{31}. The main chain CO of Arg^{789} forms a hydrogen bond with the amide group of the Gln^{61} side chain. As in uncomplexed GAP-334, the conformation of the finger loop appears to be stabilized by the interaction of Arg^{903} with the main chain carbonyl oxygens of Phe^{788}, Arg^{789}, and Ala^{790}. Arginine-903, from the most highly conserved FLR fingerprint regions of RasGAPs (^{901}FLR^{903} in $p120^{GAP}$), was found to be important for catalysis (*29*); however, its conservative replacement by Lys results in only a small reduction of GAP activity (*30, 31*). This observation together with the structure suggests an indirect role of Arg^{903} in catalysis, whereby it stabilizes the position of the crucial arginine.

In the structures of activated $G\alpha_i$ and $G\alpha_t$ and of myosin, the putative transition state mimics were identified as GDP·AlF_4^- and adenosine diphosphate (ADP)·AlF_4^-, respectively (*10, 44*). This difference is not understood and may be clarified if higher resolution data become available. AlF_3 has also been found in the transition-state mimics of nucleoside di- and monophosphate kinase structures (*45*), reflecting the ability of aluminum fluoride to form trigonal-bipyramidal complexes (*46*).

During phosphoryl transfer reactions, a partial negative charge develops. If this is on the γ-phosphate, the reaction is associative and goes through a pentavalent phosphorous intermediate. If the charge is on the leaving group, which in the hydrolysis of GTP is the β,γ-bridging oxygen atom, the mechanism is dissociative and shows a metaphosphate-like transition state (*7*). Proteins such as GAP could stabilize the transition state by neutralizing these developing charges and thus catalyze the chemical reaction. The intrinsic GTPase reaction of Ras proceeds by means of substrate-assisted catalysis in which the substrate GTP itself acts as the general (or specific) base (*6*), which would only be favorable in the case of an associative mechanism (*7*).

The structure suggests a polar interaction between the charged guanidinium group of Arg^{789} and a fluoride ligand of aluminum (Fig. 5, A and B). Because Al-F and P-O bond lengths are very similar (*46*), and because an AlF_3 trigonal base mimics the trigonal base of the transferred phosphoryl group, we assume that the observed geometry in the active site is a close mimic of that of the transition state (or intermediate) of the GTPase reaction. We can identify one axial ligand of the pentavalent aluminum as the oxygen of the GDP leaving group, the second being derived from the attacking nucleophilic water. This water molecule matches the site of Wat^{175} found in the GTP conformation of Ras (*13*) and is located within hydrogen-bonding distance to the carbonyl group of the Gln^{61} side and the Thr^{35} main chains. On the basis of the arguments put forward earlier (*7*) that residues that neutralize charges on the γ-phosphate would act anticatalytically in a dissociative mechanism, and because Arg^{789} has its strongest interaction with the fluoride ion and a weaker one with the leaving group, the arrangement of active site residues presently seen would support a mostly associative mechanism in the GTPase reaction.

The second major factor in the acceleration of the Ras-GTPase reaction by GAP appears to arise from the stabilization of the switch II region, as postulated before (*6, 10*). It has been shown both by the crystallographic analysis of Ras in the di- and triphosphate form and by nuclear magnetic resonance spectroscopy that the region around loop L4 containing Gln^{61} is very mobile with respect to the rest of the molecule (*13, 20, 36*). Glutamine-61 is invariant in Ras-like GTP-binding proteins except Rap. In the Ras·GAP-334 structure, Gln^{61} contacts one of the fluoride ions and the axial ligand derived from the nucleophilic water molecule, thereby contributing to the stability of the transition state. It gives an explanation why mutants of Gln^{61} have reduced GTPase activity and are oncogenic (*18, 19, 26, 37, 38*).

Comparison with Gα proteins. Compared with Ras and other small GTP-binding proteins, the α subunits of heterotrimeric G proteins contain an extra helical domain as an insertion into the G domain, the topological domain responsible for the biochemical properties of GTP-binding proteins. The helical domain positions an invariant arginine that appears to be critical for the GTPase reaction because its

modification by cholera toxin reduces the GTPase activity of $G\alpha_s$ (*47*) and because its mutation in $G\alpha_s$ or $G\alpha_i$ renders the proteins oncogenic (*48*). In the $G\alpha{\cdot}GDP{\cdot}AlF_4^-$ complex of both transducin and $G\alpha_{i1}$, this arginine contacts the fluorides of AlF_4^- as well as the β,γ-bridging oxygen and is thus involved in stabilization of the transition state (*10*). From the superimposition of the G domains of Ras·GAP-334 and of $G\alpha_{i1}$, the transition state mimics for the two GTPases look very similar (Fig. 5C). The guanindinium groups of the respective arginines are in a similar position, although they point into the active site from different directions. In Gα, the arginine, located in the linker connecting the helical and the G domain, is supplied in cis from the same molecule, whereas in the Ras·RasGAP system it is supplied in trans by RasGAP. The corresponding glutamine residues are also in close proximity, confirming a similar role for these conserved residues in the stabilization of the transition state and their involvement in oncogene formation (*37*, *48*).

Recently GAPs for Gα proteins, called RGS (for regulator of G protein signaling), have been described that increase the GTPase reaction rate and that have no sequence homology to RasGAPs or other GAPs for Ras-like proteins (*49*). Although the maximal rate of GTP hydrolysis has not been reported, it is estimated to be on the same order of magnitude as the maximally stimulated GTPase on Ras. Some RGS proteins bind with higher affinity to the $GDP{\cdot}AlF_4^-$ complex of Gα proteins than to the guanosine 5′-*O*-(3′-thiotriphosphate) (GTP-γ-S)–bound state, which indicates that they act by stabilizing the transition state (*50*). The recent structure determination of a complex of RGS4 with $G\alpha_{i1}{\cdot}GDP{\cdot}AlF_4^-$ (*51*) shows that RGS is a purely helical protein that contacts the switch residues of $G\alpha_{i1}$, similar to RasGAP contacting and stabilizing the switch regions of Ras.

Ras-mediated GTP hydrolysis accelerated by RasGAP is required for physiological control of a number of important signal transduction processes. Indeed, oncogenic mutants of Ras escape regulation by RasGAP. The model of the $Ras{\cdot}GDP{\cdot}AlF_3{\cdot}$ GAP-334 complex shows that GAP catalyzes the GTPase reaction by stabilizing the switch II region and by supplying a catalytic residue. In addition, it provides an explanation why mutations in both Gly^{12} and Gln^{61} activate the transforming potential of Ras: Both are in van der Waals distance from each other and from GAP in the transition state mimic. The structural view of the communication between Ras and GAP-334 may aid in the design of small molecules with the capacity to induce GTP hydrolysis on mutant oncogenic forms of Ras found in human tumors. Together with the biochemical data, it shows that for signal transduction to function properly, nature has designed Ras to be an inefficient GTPase, which can be induced to be an efficient switch-off enzyme in the presence of another signal transduction molecule.

REFERENCES AND NOTES

1. H. R. Bourne *et al.*, *Nature* **348**, 125 (1990); *ibid.* **349**, 117 (1991); D. R. Lowy and B. M. Willumsen, *Annu. Rev. Biochem.* **62**, 851 (1993).
2. M. S. Boguski and F. McCormick, *Nature* **366**, 643 (1993); A. Wittinghofer, K. Scheffzek, M. R. Ahmadian, *FEBS Lett.* **408**, 315 (1997).
3. M. Trahey and F. McCormick, *Science* **238**, 542 (1987); M. Trahey *et al.*, *ibid.* **242**, 1697 (1988); U. Vogel *et al.*, *Nature* **335**, 90 (1988).
4. G. F. Xu *et al.*, *Cell* **63**, 835 (1990); G. A. Martin *et al.*, *ibid.* **63**, 843 (1990); R. Ballester *et al.*, *ibid.* **63**, 851 (1990).
5. G. Xu *et al.*, *ibid.* **62**, 599 (1990).
6. T. Schweins *et al.*, *Nature Struct. Biol.* **2**, 36 (1995).
7. K. A. Maegley, S. J. Admiraal, D. Herschlag, *Proc. Natl. Acad. Sci. U.S.A.* **93**, 8160 (1996).
8. S. E. Neal, J. F. Eccleston, M. R. Webb, *ibid.* **87**, 3652 (1990); H. Rensland *et al.*, *Biochemistry* **30**, 11181 (1991); K. J. M. Moore, M. R. Webb, J. F. Eccleston, *ibid.* **32**, 7451 (1993).
9. R. Mittal *et al.*, *Science* **273**, 115 (1996).
10. J. Sondek, D. G. Lambright, J. P. Noel, H. E. Hamm, P. B. Sigler, *Nature* **372**, 276 (1994); D. E. Coleman *et al.*, *Science* **265**, 1405 (1994).
11. K. Scheffzek *et al.*, *Nature* **384**, 591 (1996).
12. GAP-334 and H-Ras (residues 1 through 166, missing the COOH-terminal 23 amino acids), hereafter referred to as Ras, in the GDP-bound form were expressed in *Escherichia coli* and prepared as described (*38*). For complex formation, equal amounts of both proteins (20 mg/ml in 20 mM Hepes, pH 8) were mixed along with 2 mM $AlCl_3$ and 20 mM NaF. Crystals were grown by the hanging drop method with 15 to 20% polyethylene glycol 3350 in 100 mM Hepes (pH 8) with 20 mM ammonium sulfate and 20 mM NaF as the precipitant, and improved by seeding protocols similar to those described by K. Scheffzek *et al.* [*Proteins Struct. Funct. Genet.* **27**, 315 (1997)] together with 100 mM guanidine hydrochloride as additive. The crystals belong to the monoclinic space group $P2_1$ with unit cell dimensions a = 71.9 Å, b = 41.1 Å, c = 89 Å, α = 90°, β = 108.4°, and γ = 90°; they contain one RasGAP-334 complex in the asymmetric unit. Few crystals diffracted to resolutions higher than 3 Å. A data set from a single crystal (cooled to 4°C) was collected by the rotation method with mirror-focused x-rays from a rotating anode (Elliott GX18; 35 kV/50 mA) and a Siemens/Nicolett area detector for data recording. Space group determination, data processing, and scaling were done with the programs XDS and XSCALE [W. Kabsch, *J. Appl. Crystallogr.* **26**, 795 (1993)]. We used data to 2.5 Å resolution; the completeness between 2.6 and 2.5 Å is 65%; 2027 reflections of nonpositive intensity were excluded from the refinement.
13. E. F. Pai *et al.*, *EMBO J.* **9**, 2351 (1990); E. F. Pai *et al.*, *Nature* **341**, 209 (1989).
14. A. T. Brünger, *X-PLOR*, version 3.8 (Yale University, New Haven, CT, 1996).
15. T. A. Jones, J. Y. Zou, S. W. Cowan, M. Kjelgaard, *Acta Crystallogr.* **A47**, 110 (1991).
16. J. Janin and C. Chothia, *J. Biol. Chem.* **265**, 16027 (1990).
17. H. Adari, D. R. Lowy, B. M. Willumsen, C. J. Der, F. McCormick, *Science* **240**, 518 (1988); C. Calés, J. F. Hancock, C. J. Marshall, A. Hall, *Nature* **332**, 548 (1988); M. S. Marshall and L. A. Hettich, *Oncogene* **8**, 425 (1993); M. S. A. Nur-E-Kamal, A. Sizeland, G. D'Abaco, H. Maruta, *J. Biol. Chem.* **267**, 1415 (1992).
18. M. S. Marshall, *Trends Biochem. Sci.* **18**, 250 (1993).
19. P. Polakis and F. McCormick, *J. Biol. Chem.* **268**, 9157 (1993); P. Morcos *et al.*, *Mol. Cell. Biol.* **16**, 2496 (1996); M. C. Parrini, A. Bernardi, A. Parmeggiani, *EMBO J.* **15**, 1107 (1996).
20. M. V. Milburn *et al.*, *Science* **247**, 939 (1990).
21. N. Nassar *et al.*, *Nature* **375**, 554 (1995).
22. J. F. Eccleston *et al.*, *J. Biol. Chem.* **268**, 27012 (1993).
23. M. R. Ahmadian *et al.*, *ibid.* **271**, 16409 (1996).
24. A. Wittinghofer and N. Nassar, *Trends Biochem. Sci.* **21**, 488 (1996).
25. M. H. Tsai, A. Hall, D. W. Stacey, *Mol. Cell. Biol.* **9**, 5260 (1989); M. Golubic *et al.*, *EMBO J.* **10**, 2897 (1991); J. Serth, A. Lautwein, M. Frech, A. Wittinghofer, A. Pingoud, *ibid.*, p. 1325.
26. G. Bollag and F. McCormick, *Nature* **351**, 576 (1991).
27. B. A. Sermon, J. F. Eccleston, R. H. Skinnert, P. N. Lowe, *J. Biol. Chem.* **271**, 1566 (1996).
28. U. Krengel *et al.*, *Cell* **62**, 539 (1990).
29. G. G. Brownbridge *et al.*, *J. Biol. Chem.* **268**, 10914 (1993).
30. R. H. Skinner *et al.*, *ibid.* **266**, 14163 (1991).
31. M. R. Ahmadian *et al.*, unpublished data; M. R. Ahmadian, P. Steege, K. Scheffzek, A. Wittinghofer, *Nature Struct. Biol.*, in press.
32. Y. Li *et al.*, *Cell* **69**, 275 (1992).
33. P. Poullet, B. Lin, K. Esson, F. Tamanoi, *Mol. Cell. Biol.* **14**, 815 (1994).
34. L. Wiesmüller and A. Wittinghofer, *J. Biol. Chem.* **267**, 10207 (1992).
35. S. Mori *et al.*, *ibid.* **270**, 28834 (1995).
36. P. J. Kraulis, P. J. Domaille, S. L. Campbell-Burk, T. V. Aken, E. D. Laue, *Biochemistry* **33**, 3515 (1994).
37. C. J. Der *et al.*, *Cell* **44**, 167 (1986).
38. P. Gideon *et al.*, *Mol. Cell. Biol.* **12**, 2050 (1992).
39. G. G. Privé *et al.*, *Proc. Natl. Acad. Sci. U.S.A.* **89**, 3649 (1992).
40. K. Scheffzek, unpublished observation.
41. P. H. Seeburg *et al.*, *Nature* **312**, 71 (1984).
42. J. B. Gibbs, M. D. Schaber, W. J. Allard, I. S. Sigal, E. M. Scolnick, *Proc. Natl. Acad. Sci. U.S.A.* **85**, 5026 (1988).
43. S. M. Franken *et al.*, *Biochemistry* **32**, 8411 (1993).
44. A. J. Fisher *et al.*, *ibid.* **34**, 8960 (1995).
45. Y.-W. Xu, S. Moréra, J. Janin, J. Cherfils, *Proc. Natl. Acad. Sci. U.S.A.* **94**, 3579 (1997); I. Schlicting and J. Reinstein, *Biochemistry*, in press.
46. M. Chabre, *Trends Biochem. Sci.* **15**, 6 (1990).
47. C. van Dop, M. Tsubokawa, H. R. Bourne, J. Ramachandran, *J. Biol. Chem.* **259**, 696 (1984).
48. J. Lyons *et al.*, *Science* **249**, 655 (1990); C. A. Landis *et al.*, *Nature* **340**, 692 (1989).
49. H. K. G. Dohlman and J. Thorner, *J. Biol. Chem.* **272**, 3871 (1997).
50. D. M. Berman, T. Kozasa, A. G. Gilman, *ibid.* **271**, 27209 (1996); N. Watson, M. E. Linder, K. M. Druey, J. H. Kehrl, K. J. Blumer, *Nature* **383**, 172 (1996).
51. J. J. G. Tesmer, D. M. Berman, A. G. Gilman, S. R. Sprang, *Cell* **89**, 251 (1997).
52. P. J. Kraulis, *J. Appl. Crystallogr.* **24**, 946 (1991).
53. E. A. Merrit and W. F. Anderson, *Acta Crystallogr.* **D50**, 219 (1994).
54. W. Kabsch and C. Sander, *Biopolymers* **22**, 2577 (1983).
55. Single-letter abbreviations for the amino acid residues are as follows: A, Ala; C, Cys; D, Asp; E, Glu; F, Phe; G, Gly; H, His; I, Ile; K, Lys; L, Leu; M, Met; N, Asn; P, Pro; Q, Gln; R, Arg; S, Ser; T, Thr; V, Val; W, Trp; and Y, Tyr.

56. We thank A. Becker, I. Schlichting, I. Vetter, M. Geyer, A. Scherer, and A. Lavie for helpful discussions, H. Wagner for maintenance of the x-ray facilities at the Max-Planck-Institut für medizinische Forschung Heidelberg, R. Schebaum for secretarial assistance, and K. Holmes for continuous support. Supported by the Peter and Traudl Engelhorn Stiftung (Germany) and the National Neurofibromatosis Foundation (United States) (K.S.). The coordinates have been submitted to the Brookhaven data base, accession number 1WQ1.

1 May 1997; accepted 20 June 1997